Available online at www.sciencedirect.com
SCIENCE DIRECT®
Nuclear Instruments and Methods in Physics Research A 555 (2005) 270–281
NUCLEAR INSTRUMENTS & METHODS IN PHYSICS RESEARCH Section A
www.elsevier.com/locate/nima

Performances and potentialities of a $LaCl_3$:Ce scintillator

R. Bernabei[a,*], P. Belli[a], F. Montecchia[a], F. Nozzoli[a], A. d'Angelo[b,c], F. Cappella[b], A. Incicchitti[b], D. Prosperi[b], S. Castellano[d,e], R. Cerulli[d], C.J. Dai[f], V.I. Tretyak[g]

[a]*Dipartimento di Fisica, Università di Roma "Tor Vergata", and INFN, Sezione di Roma2, I-00133 Rome, Italy*
[b]*Dipartimento di Fisica, Università di Roma "La Sapienza" and INFN, Sezione di Roma, I-00185 Rome, Italy*
[c]*Scuola di Specializzazione in FISICA SANITARIA, Università di Roma "Tor Vergata", I-00133 Rome, Italy*
[d]*INFN, Laboratori Nazionali del Gran Sasso – 67010 Assergi (AQ), Italy*
[e]*Università degli Studi dell'Aquila, I-67000 L'Aquila, Italy*
[f]*IHEP, Chinese Academy, P.O. Box 918/3, Beijing 100039, China*
[g]*Institute for Nuclear Research, MSP 03680 Kiev, Ukraine*

Received 26 August 2005; accepted 22 September 2005
Available online 18 October 2005

Abstract

The performances and the potentialities of applications of a $LaCl_3$:Ce scintillator have been investigated deep underground in the Gran Sasso Laboratory of the I.N.F.N. In particular, the light response, the α/β ratio, the α/β discrimination capability and the radioactive contaminations have been studied. The results of an experimental search for spontaneous cluster decay in La isotopes are also presented.

PACS: 29.40.Mc; 23.60.+e; 23.70.+j

Keywords: $LaCl_3$:Ce crystal scintillator; α/β Ratio; Cluster decay

1. Introduction

A large deal of interest has been devoted by DAMA to investigate on new kinds of scintillators for various applications; in particular, the recently developed $LaCl_3$:Ce scintillator has been considered and its scintillation and background characteristics have been studied.

In literature several investigations have been carried out on various $LaCl_3$:Ce prototypes [1–5]. The emission and excitation characteristics of $LaCl_3$:Ce were measured at $\simeq$ 8 K under ultraviolet excitation [6] and in particular, in Ref. [1] the light response for different Ce concentrations has been studied. They support for this scintillator a good linearity with energy (at low energy the maximum deviation less than 5%) [7] measuring a scintillation light yield typically of about 49 000 ph/MeV, while the photoelectron yield is about 70–90% with the respect to NaI(Tl) [2]. When doped with $\simeq$10% Ce the $LaCl_3$ has a fast principal decay time constant: 26 ns [3], allowing to obtain a fast time response; a good timing resolution was also found comparable to that of BaF_2 scintillator. In Ref. [2] the response of a $LaCl_3$:Ce has also been studied as a function of the temperature (from -65 to 100 °C) showing the potential interest for applications at high temperature.

The $LaCl_3$:Ce has a maximum emission wavelength at 350 nm and a second peak in the range 420–440 nm depending on Ce concentration. The density is typically of order of 3.8 g/cm^3 and the refractive index at maximum emission wavelength $\simeq$ 1.9; it is hygroscopic [2] and due to the high Z of La and Ce atoms it is a good γ, β detector.

All these qualities have gained our attention and in this paper the results obtained by investigating deep underground (about 3600 m w.e.) at the Gran Sasso National Laboratory of I.N.F.N. the features of a $LaCl_3$:Ce scintillator produced by *Saint Gobain crystals and detectors* are reported.

*Corresponding author. Tel.: 390672594542; fax: 390672594542.
E-mail address: rita.bernabei@roma2.infn.it (R. Bernabei).

0168-9002/$ - see front matter © 2005 Elsevier B.V. All rights reserved.
doi:10.1016/j.nima.2005.09.030

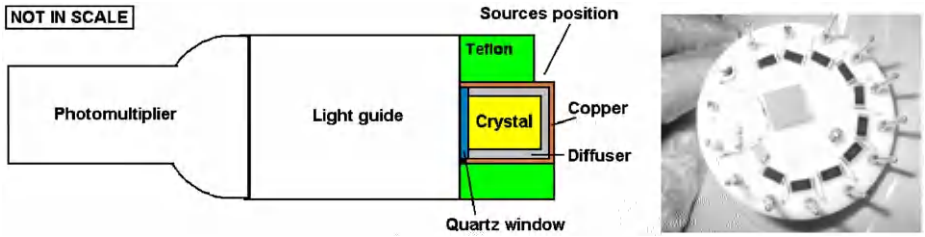

Fig. 1. *Left:* schematic view not in scale of the $LaCl_3$:Ce detector. See text. *Right:* a typical DAMA voltage divider with SMD components; it is mounted on a teflon disk to be directly connected on the flying leads of the PMT.

The measurements described here have been performed in the DAMA/R&D apparatus, which is a multipurpose set-up devoted to tests on detectors' and PMTs low background prototypes and to small scale experiments investigating various processes such as $\beta\beta$ decay modes in ^{40}Ca, ^{46}Ca, ^{48}Ca, ^{106}Cd, ^{130}Ba, ^{136}Ce, ^{138}Ce, ^{142}Ce [8–13].

Here the light response, the α/β ratio, the α/β discrimination capability and the radioactive contaminations have been investigated. Moreover, the energy distribution of the background, arising from such contaminations, has been accounted by a Monte Carlo simulation based on the EGS4 code [14]. The data have been then used to investigate some possible cluster decays in La isotopes.

2. The experimental set-up

The used detector is a $LaCl_3$:(8.5±1.0%)Ce (25.4 ± 0.2 mm in diameter by 25.4 ± 0.2 mm length). It has a density $\rho = (3.86 \pm 0.01)\,g/cm^3$ [15] corresponding to a mass of (49.7 ± 1.3) g. The crystal is encapsulated in a OFHC copper housing 1 mm thick; between copper and crystal there are about 2.5 mm of diffuser. The optical window is made of quartz. The detector is a commercial crystal and no particular selection of crystal materials has been pursued; in fact, one of the goal of this work was the identification of the starting levels of residual contaminations in such a detector.

The crystal scintillator has been viewed by a low background photomultiplier (PMT) EMI9265-B53/FL ($\simeq$ 30% quantum efficiency at 380 nm) through a Tetrasil-B light guide (7.6 cm diameter 10 cm long) to even further reduce the residual contribution from the low background PMT (see Fig. 1). In order to reduce further the environmental radioactivity, the voltage divider has directly been mounted on the flying leads of the PMT over a teflon disk by using miniaturized SMD capacitors and resistors, which are soldered by low radioactive lead and special resin (see Fig. 1).

The experimental configuration has been put inside a low-radioactivity sealed copper box fulfilled with low radioactive Cu bricks. It is installed in the center of a low-radioactivity passive shield of Cu/Pb/Cd-foils/polyethylene/paraffin. The inner copper box is flushed with high-purity (HP) Nitrogen gas and kept in slightly over-pressure with the respect to the external environment. Also the whole shield is sealed and maintained in the HP Nitrogen atmosphere (see Fig. 2). The low background Cu and Pb of the passive shield have suitably been etched and maintained in HP Nitrogen atmosphere until the installation.

Fig. 2. Shield of the DAMA/R&D set-up and the authomatic system to close it.

The electronic chain is summarized in Fig. 3.

In particular, three charge ADC channels are acquired (with a 120 ns gate) to collect energy information in different energy ranges; moreover, the signals from the PMT are also recorded by a 160 MSa/s Transient Digitizer, TD, over a time window of 3125 ns.

3. Measured main features of the $LaCl_3$:Ce detector

The light response, the linearity, the energy resolution, the α/β ratio and the α/β discrimination capability have been studied. The main radioactive contaminations in the background have been quantified.

3.1. Calibrations

The energy calibrations have been performed in two different experimental conditions: (i) crystal directly coupled to the PMT; (ii) crystal coupled to PMT through the light guide (since this last one is the experimental

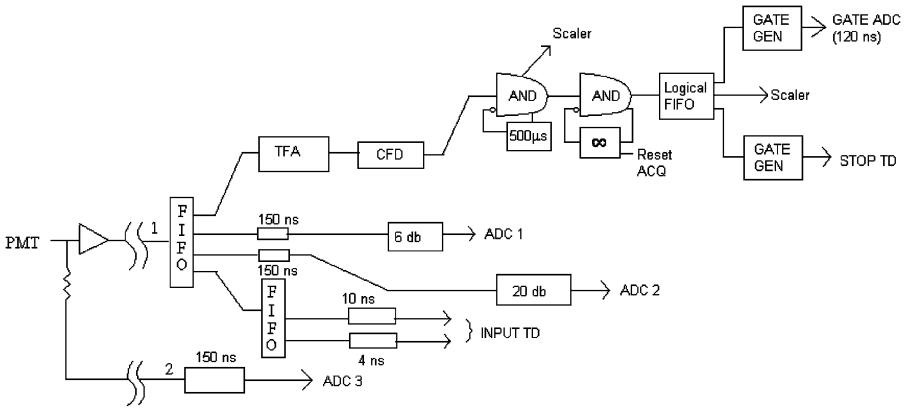

Fig. 3. Scheme of the electronic chain.

condition of the production runs). The measured energy distributions are shown in Figs. 4 and 5, respectively.

The behaviours of the energy calibrations are shown in Fig. 6 (a). The energy calibration is (0.6090 ± 0.0003) ch/keV in case (i) and (0.4061 ± 0.0006) ch/keV in case (ii); thus, the collected light is reduced by about 33% when using that light guide on $LaCl_3$:Ce. Moreover, the energy resolution is in the first case: $\sigma/E = 0.003 + 0.51/\sqrt{E[keV]}$, and in the second case: $\sigma/E = 0.004 + 0.59/\sqrt{E[keV]}$, respectively; they are shown in Fig. 6 (b). As example, one gets $FWHM/E = 5.4\%$ at 662 keV γ quanta of ^{137}Cs without using light guide.

By comparing the measured energy calibration spectra with those obtained by a devoted Monte Carlo full simulation, the number of photoelectrons/keV has been derived: 7.2 ± 1.0 for the first case and 4.8 ± 1.0 for the second case, respectively.[1]

3.2. Pulse shape discrimination capability

The pulse shape discrimination capability between α and $\gamma(\beta)$ particles has been investigated by studying the pulses recorded by Transient Digitizer. Various analysis approaches can be pursued; here we have exploited in particular the optimal digital filter method [16].

To obtain the numerical characteristic of the $LaCl_3$:Ce scintillation signal, namely the shape indicator (SI), the following formula has been applied for each pulse: $SI = \sum_k f(t_k) \times P(t_k)$, where k identifies the TD time channel in the time interval 44–200 ns. Moreover, $f(t)$ is the digitized amplitude of a given signal normalized to its area. The weight function $P(t)$ is defined as: $P(t) = f_\alpha(t) - f_\gamma(t)$, where $f_\alpha(t)$ and $f_\gamma(t)$ are the reference pulse shapes for α particles and γ quanta, respectively. In particular, $f_\alpha(t)$ has been obtained by averaging about 40 000 individual events in the energy range 1800–2400 keV, where the analysis of the behaviour of the measured background assures the presence of only α particles' events from U and Th chains. To obtain instead $f_\gamma(t)$, about 40 000 individual events of energy around 1500 keV have been averaged; in fact, the events below 1600 keV can be mainly ascribed to β and EC decays of ^{138}La (natural abundance: 0.0902%).

The scatter plot of the shape indicator versus energy for the deep underground background measurements with the used $LaCl_3$:Ce crystal is depicted in Fig. 7.

The population of the α events is slightly shifted relatively to that of the $\gamma(\beta)$ events. As it is visible in the inset of Fig. 7, the distributions of the shape indicator for $\gamma(\beta)$ and α events are well described by Gaussian functions. In particular, we obtain for the reference pulses: $SI_\alpha = 1.88 \times 10^{-3}$ with standard deviation $\sigma_\alpha = 0.03 \times 10^{-3}$ and for $SI_\gamma = 1.99 \times 10^{-3}$ with standard deviation $\sigma_\gamma = 0.04 \times 10^{-3}$.

The results of this analysis are in substantial agreement with the possibility of statistical pulse shape discrimination in $LaCl_3$:Ce as already suggested in Ref. [17].

3.3. Study on correlated events: α–α and Bi–Po events

An analysis of the events time correlated in the TD time window—for the data collected deep underground during 70.2 h—has been carried out. Examples of double pulses in the TD time window are shown in Fig. 8.

As first, we have investigated α–α time correlated events in the TD time window; see Fig. 8 (c) and (d). They can be produced in particular by α decay of ^{219}Rn into ^{215}Po followed by ^{215}Po α decay ($T_{1/2} \sim 1.781$ ms) into ^{211}Pb (isotopes of the ^{235}U chain) and can be identified by applying the shape indicator method.

Note that when considering only α particles the mean rate measured by the detector is $\simeq 0.37$ Hz, i.e.—consider-

[1]Note that a lower limit on the number of photoelectrons, $N_{\rm phe}$, can be obtained by using the very simple formula: $\sigma/E \geqslant \sqrt{N_{phe}}/N_{\rm phe}$, which however does not account for all the factors contributing to the broadening of the energy resolution such as, for example, a not perfect uniformity of the detector, the broadening due to the charge distribution of the pulse of each photoelectron, the light propagation in the specific detector, etc.

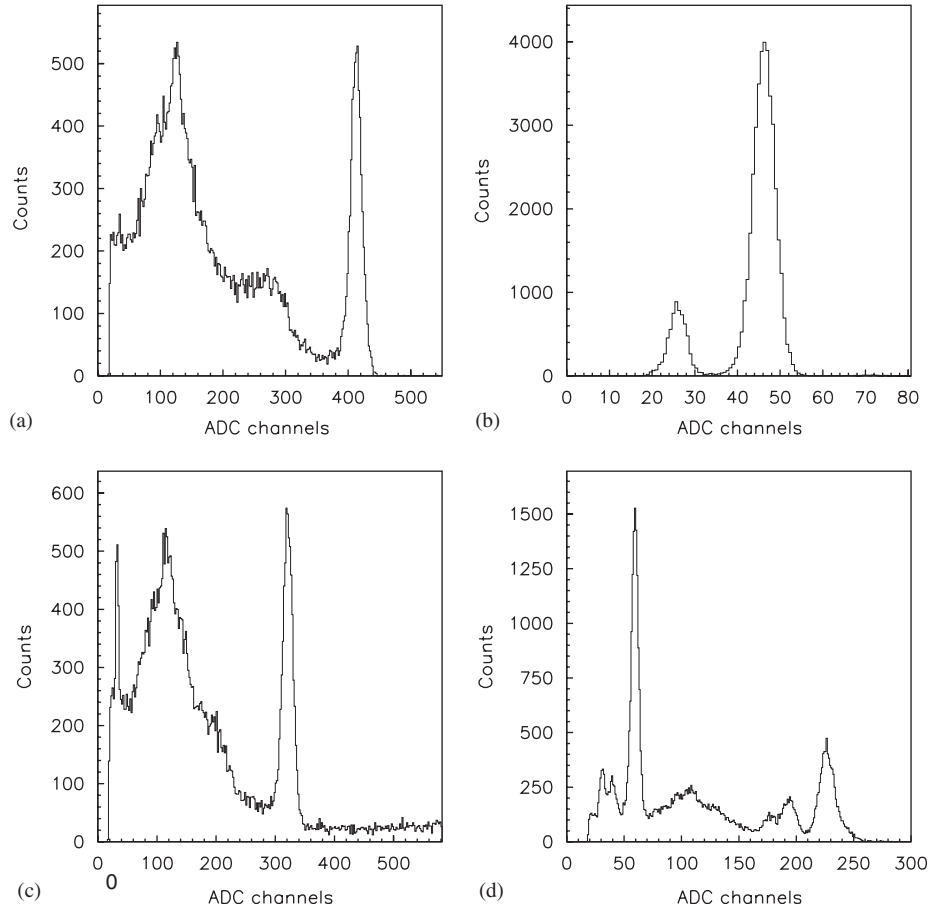

Fig. 4. Energy distributions measured by the $LaCl_3$:Ce detector with the PMT directly coupled to its optical window by using the following γ sources: (a) ^{137}Cs with peak at 662 keV; (b) ^{241}Am with peak at 59.5 keV; (c) ^{22}Na with peak at 511 keV (the peak at 1275 keV is here out of scale); (d) ^{133}Ba with peaks at 81 keV and ~356 keV.

ing an effective TD time window of 2400 ns—the expected α–α random coincidences are 0.03 events/day to be compared with the measured rate of (6.2 ± 1.4) events/day.

In Fig. 9 the *SI* values of the two characteristic pulses of α–α events are shown as a function of the corresponding energy.[2] In particular, the events corresponding to the first pulse in the time window (full circles) have a mean energy of (2.213 ± 0.026) MeV and are due to the ^{219}Rn α decay (79.4% α of 6.819 MeV, 12.9% α of 6.553 MeV and 7.5% α of 6.425 MeV). As regards the events corresponding to the second pulse (empty circles) they have a mean energy of (2.537 ± 0.023) MeV and are due to the ^{215}Po α decay ($\simeq$ 100% α of 7.386 MeV). Thus, from the α–α events it is possible to derive the α/β ratio by comparing the detected α energy on the energy scale calibrated with γ sources and the real α energy. In our detector $\alpha/\beta = 0.328 \pm 0.004$ for the ^{219}Rn peak and 0.343 ± 0.003 for the ^{215}Po peak; these values are largely consistent with the value of (0.33 ± 0.01) for the ^{214}Po α of 7.686 MeV given in Ref. [18]. Moreover, from the analysis of these events, the contamination of ^{235}U in the detector can be quantified, considering that the detection efficiency of α–α events in 2400 ns time window is 9.34×10^{-2}%.Therefore, an activity of $(66 \pm 16) \times 10^2$ dec/day can be estimated, that is when assuming the ^{235}U chain in equilibrium: (19 ± 5) ppb of ^{235}U.

Moreover, we have also analyzed the class of the so-called Bi–Po events. A Bi–Po event from ^{232}Th chain is given by the β decay of ^{212}Bi into ^{212}Po followed by the ^{212}Po α decay ($T_{1/2}$~299 ns), while a Bi–Po event from ^{238}U chain is given by the β decay of ^{214}Bi into ^{214}Po followed by the ^{214}Po α decay ($T_{1/2}$~164 μs). Also these events can be identified by studying the pulse information recorded by the TD: however, considering also in this case an effective TD time window of 2400 ns, Bi–Po events from ^{232}Th chain are mostly recorded (see Fig. 8 (a)). In particular, the detection efficiency is 99.6% for Bi–Po events of ^{232}Th chain and 1.01% for those of ^{238}U chain. In the exposure of 70.2 h only two β–α events have been identified from the *SI* and the energies of the two pulses. Note that in this case the random coincidences are not negligible, since their rate is 3.9×10^{-6} Hz; therefore, in 70.2 h the expected random coincidences are 0.99. The two events have

[2]It is worth to note that the detected energy of α particles is given in the following in keV (or MeV) electron equivalent since it refers to an energy scale obtained by γ sources calibrations.

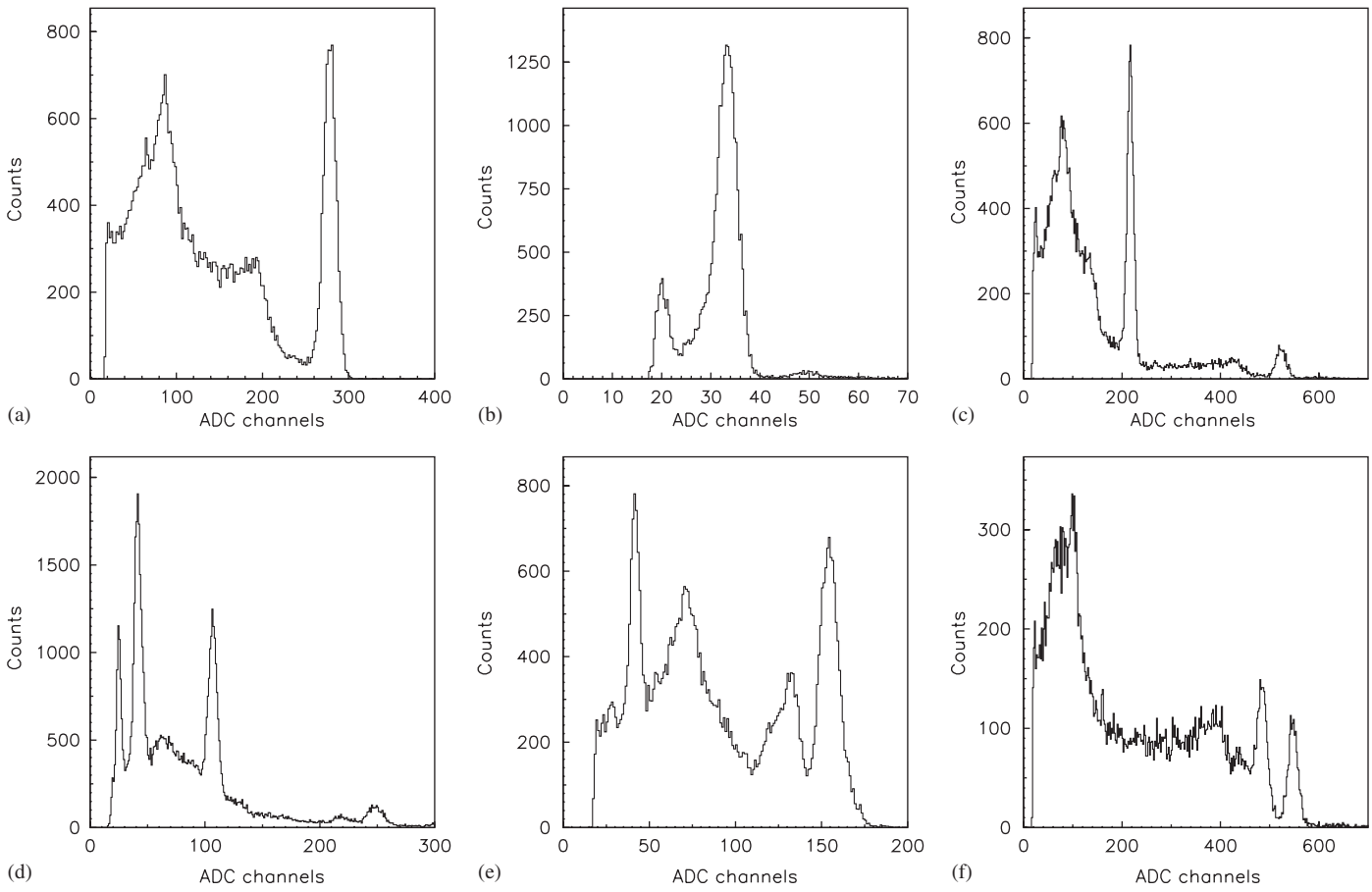

Fig. 5. Energy distributions measured by the $LaCl_3$:Ce detector with the PMT coupled to the optical window of the detector through the light guide by using the following γ sources: (a) ^{137}Cs with peak at 662 keV; (b) ^{241}Am with peak at 59.5 keV; (c) ^{22}Na with peaks at 511 and 1275 keV; (d) ^{228}Th with peaks at 239 and 583 keV (sources ^{228}Th set at ~10 cm from the detector); (e) ^{133}Ba with peaks at 81 and ~356 keV, in this case the source was positioned in a slightly different way than in the other cases; (f) ^{60}Co with peaks at 1173 and 1332 keV.

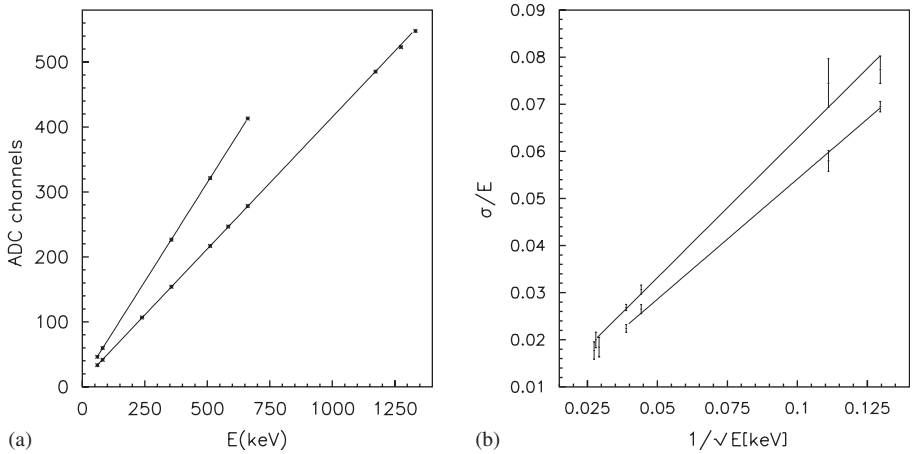

Fig. 6. (a) Linearity of the $LaCl_3$:Ce crystal, without (upper line) and with (lower line) light guide. The points correspond to the γ photopeaks in the Fig. 4 for the calibration without light guide and in Fig. 5 for the calibration with light guide. (b) Behaviours of σ/E measured with the $LaCl_3$:Ce detector without (lower line) and with (upper line) light guide, respectively; in the case with light guide only 7 of the 10 γ peaks present in Fig. 5 have been considered. In fact, for ^{228}Th peaks the source was at ~10 cm from detector, while the peak at ~356 keV from ^{133}Ba is due to the superimposition of more γ's. In the case without light guide only 4 peaks of Fig. 4 have been taken into account not considering for the same reason the ~356 keV peak from ^{133}Ba.

energies: $E^1_\beta = 162$ keV, $E^1_\alpha = 1905$ keV the first one and $E^2_\beta = 1268$ keV, $E^2_\alpha = 3268$ keV the second one. The energy E^2_α is high and could be ascribed to a ^{212}Bi–^{212}Po Bi–Po event with an α of 8785 keV; in this case the α/β ratio is $\simeq 0.37$, suggesting an energy dependence of this quantity (see also later).

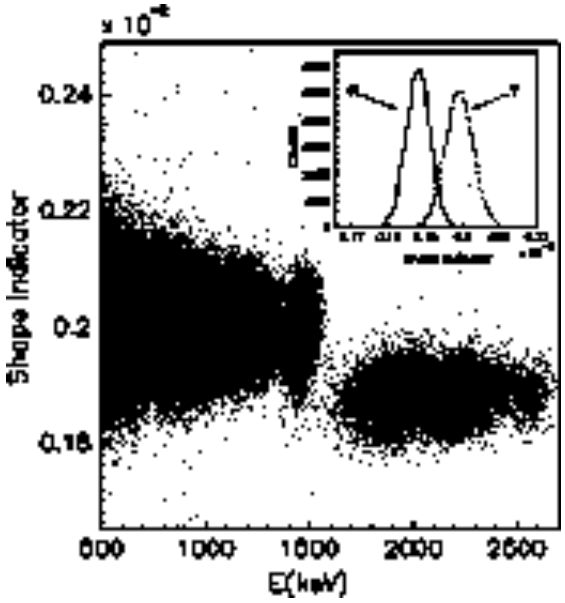

Fig. 7. Scatter plot of the shape indicator *SI* (see text) versus energy for the deep underground background measurements with the $LaCl_3$:Ce scintillation detector. The α events are in the region above $\simeq 1600$ keV, while the γ (β) events are below this energy. In the inset: the distributions of the shape indicator measured for γ quanta (corresponding to energies around 1500 keV) and for α events (corresponding to the 1800–2400 keV energy interval).

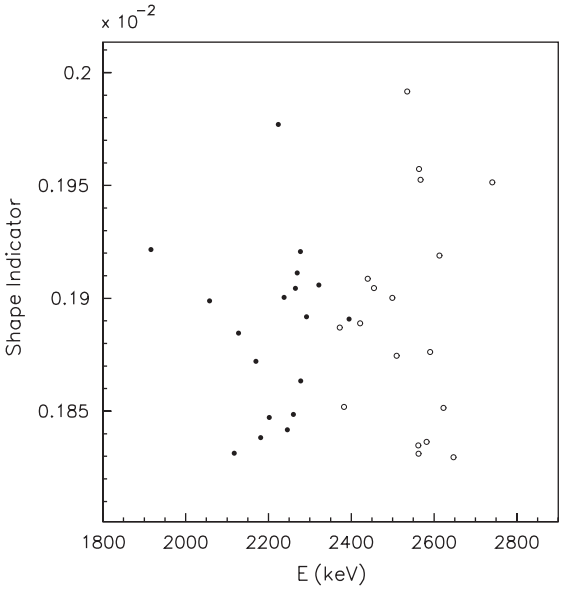

Fig. 9. *SI* values versus energy obtained for α–α events. The events with energy $\sim$2.2 MeV (full circles) are due to the first pulse in the time window of the TD and are due to α decay of ^{219}Rn. The events at $\sim$2.5 MeV (empty circles) are due to the second pulse in the time window of the TD, due to α decay of ^{215}Po.

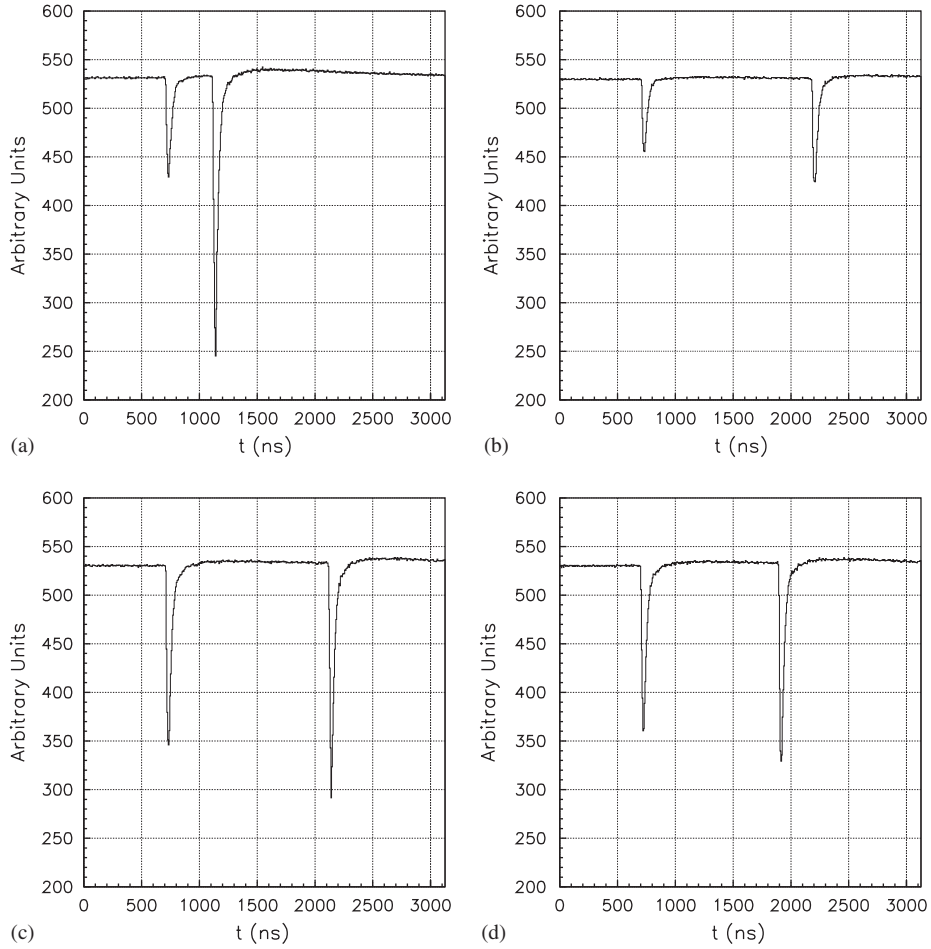

Fig. 8. Examples of time correlated events in the TD time window: identified as Bi–Po, (a); identified as random coincidence, (b); identified as α–α events from ^{219}Rn–^{215}Po–^{211}Pb, (c) and (d).

From the Bi–Po events it is also possible to estimate the ^{238}U and ^{232}Th contamination inside the $LaCl_3$:Ce detector. An upper limit of 4.45 events (90% C.L.) [19] for the Bi–Po events from both the ^{238}U and ^{232}Th chains can be set, i.e.:

$$a_{^{212}\mathrm{Bi}-^{212}\mathrm{Po}} < 1.5\,\mathrm{dec/day}\ (90\%\ \mathrm{C.L.}) \quad (1)$$

$$a_{^{214}\mathrm{Bi}-^{214}\mathrm{Po}} < 150\,\mathrm{dec/day}\ (90\%\ \mathrm{C.L.}). \quad (2)$$

Considering the chains in equilibrium, it results in ^{232}Th and ^{238}U contaminations,

$$C_{^{232}\mathrm{Th}} < 88\,\mathrm{ppt}\ (90\%\ \mathrm{C.L.}) \quad (3)$$

$$C_{^{238}\mathrm{U}} < 2.8\,\mathrm{ppb}\ (90\%\ \mathrm{C.L.}). \quad (4)$$

Let us comment the contaminations of ^{238}U with the respect to ^{235}U in the $LaCl_3$:Ce crystal. Typically, considering the halflife and the natural abundance of these two isotopes, the activity of ^{238}U should be about 20 times larger than that of ^{235}U. This is not the case in $LaCl_3$:Ce as obtained here and by other authors [20,18,5]; see also later.

4. Further analyses on the $LaCl_3$:Ce radioactive contaminations

The background spectrum of the $LaCl_3$:Ce crystal measured deep underground in the low background set-up is depicted in Fig. 10.

The measured background is fully dominated by the internal residual contaminants; in particular, as already mentioned, the events below $\simeq$ 1600 keV are mainly due to the radioactive decays of ^{138}La present in the natural La, while the events above $\simeq$ 1600 keV are due to α particles mainly from ^{235}U decay chain.

In the analysis of the background, presented in the following, we have simulated the contribution of each identified contaminant to the experimental energy spectrum by using the EGS4 code [14]; for the α particles it has been assumed that their whole energies are released inside the detector.

4.1. Contribution from ^{235}U decay chain

As suggested from the previous analysis on the α–α events, an important contribution to the measured background can be ascribed to isotopes from the ^{235}U decay chain.

As a first step, let us assume this decay chain at equilibrium and point our attention out on the experimental energy distribution of the α events (see Fig. 11). In this way, we can ascribe the structure at ~2200 keV to the α decays of ^{219}Rn ($Q_\alpha = 6950$ keV), as already pointed out also by the previous study on $\alpha-\alpha$ events, and to those of the ^{211}Bi ($Q_\alpha = 6750$ keV). Moreover, the α/β ratio estimated above allows to ascribe the peak at ~1900 keV

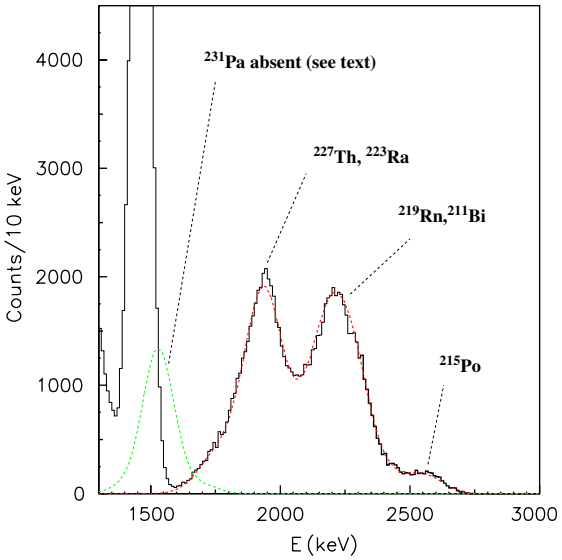

Fig. 11. Comparison between the expected energy distribution by using the *best-fit* parameters (dashed line) and the experimental one (continuous histogram). Here is also shown (light dashed line) the expected distribution for the α decay of ^{231}Pa in case the same activity for the other isotopes of the chain is assumed (see text). The absence of this peak in the experimental data can be explained if the chain is broken between ^{231}Pa ($T_{1/2} = 3.276 \times 10^4$ yr) and ^{227}Ac ($T_{1/2} = 21.8$ yr).

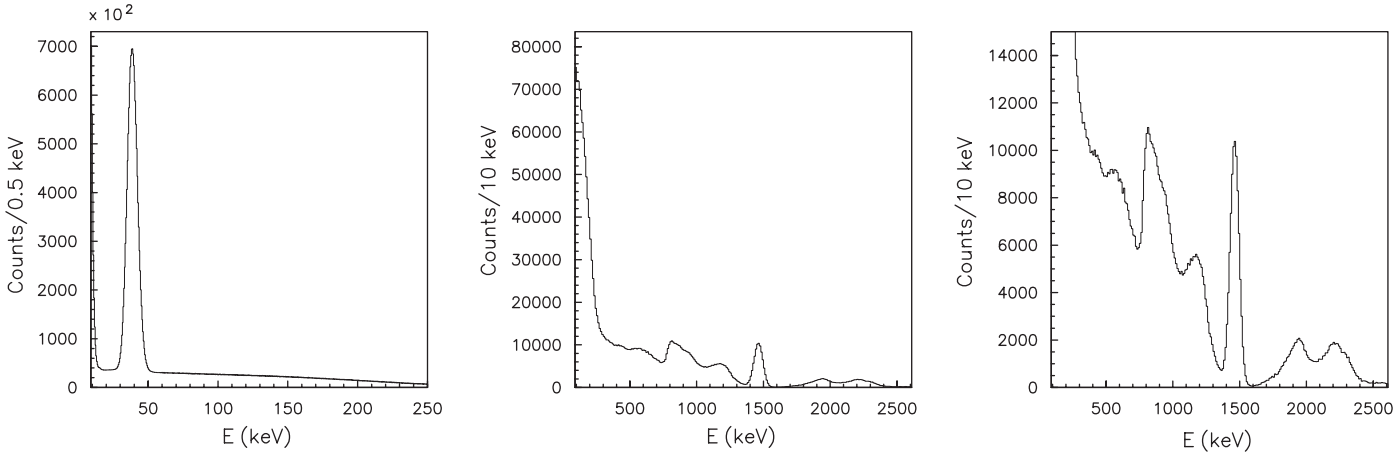

Fig. 10. Background energy distribution measured by the $LaCl_3$:Ce detector in the low background DAMA/R&D set-up at LNGS. The lowest energy distribution refers to 493 h of data taking, while the other two regions to 70.2 h.

to the α decays of the ^{223}Ra ($Q_\alpha = 5980$ keV) and of ^{227}Th ($Q_\alpha = 6150$ keV). It is worth to note that in this energy distribution the expected peak at ~2600 keV—see Fig. 9—from the α decay of ^{215}Po is strongly suppressed (~85%) because of the short halflife of the ^{215}Po ($T_{1/2} \simeq 1.781$ ms) with the respect to the DAQ dead-time; in fact, most of its decays occur during the DAQ dead time (~5 ms) after the ^{219}Rn decay.

As regards the α decay of ^{231}Pa ($Q_\alpha = 5150$ keV), which is the third element in the ^{235}U chain, considering the previous estimates of the α/β ratio, it should induce a peak at energy ~1600 keV. As it can be seen, there is no evidence for it in the experimental energy spectrum; this can be explained by abandoning the assumption of chain in equilibrium and considering that it is broken between ^{231}Pa ($T_{1/2} = 3.276 \times 10^4$ yr) and ^{227}Ac ($T_{1/2} = 21.8$ yr).

Starting from these preliminary considerations, a further analysis of events due to α contaminations has been performed by realizing a Monte Carlo simulation of the α decays of ^{227}Th, ^{223}Ra, ^{219}Rn, ^{215}Po and ^{211}Bi (because of the above proved absence of ^{231}Pa). The full decay scheme of each isotope has been considered and for each event the total energy, E, released in the detector has been calculated. In particular, for the α particles the α/β ratio has been written as: $\alpha/\beta = a_0 + a_1 \times E_\alpha$, expliciting its linear dependence on the α deposited energy, E_α.

The expected energy distribution, $S_{a_0,a_1,c_1,c_2,N_1,N_2}(E)$, is a linear combination of the energy distribution obtained by the previous simulations and is function of 6 parameters. The a_0 and a_1 parameters are related to the α/β ratio; the c_1 and c_2 are related to the energy resolution: $\sigma/E = c_1 + c_2/\sqrt{E}$. The parameter N_1 represents the number of decays due to ^{227}Th (and, therefore, to its daughters: ^{223}Ra, ^{219}Rn and ^{211}Bi, which are considered at equilibrium) and N_2 is the number of decays due to ^{215}Po acquired by the DAQ system; we expect $N_2 \ll N_1$ because of the DAQ dead time as mentioned above.

The fit has been performed by minimizing in the energy interval 1600–2800 keV the function:

$$Z^2 = \sum_k \frac{(S_{a_0,a_1,c_1,c_2,N_1,N_2}(E_k) - O_k)^2}{O_k} \quad (5)$$

with the respect to the free parameters a_0, a_1, c_1, c_2, N_1 and N_2, where E_k is the mean energy in the k bin and O_k the experimental counts measured in the k bin.

Using the *best-fit* parameters the energy distribution shown in Fig. 11 (dashed line) is obtained. The agreement with the experimental distribution (continuous histogram) is very good.

Moreover, by using the *best-fit* value of the parameter N_1 we can estimate the activity of the single components of the radioactive chain (assumed in equilibrium): $a = N_1/T_{acq} = (77 \pm 1) \times 10^2$ dec/day, value that is in agreement with that previously estimated with the analysis of the α–α events. Furthermore, from the *best-fit* values of the parameters N_1 and N_2 it follows that only N_2/N_1 ~13% of the ^{215}Po decays is acquired, confirming our previous estimation. As a by-product, we can also obtain from the *best-fit* parameters a_0 and a_1 the ratio:

$$\alpha/\beta = 0.187 + 0.0216 \times E_\alpha[MeV] \quad (6)$$

that is valid for α particles with energy E_α between 6 and 7.5 MeV and is well in agreement with estimates given above.

Assuming for the α decay of ^{231}Pa the same activity as the other isotopes of the chain and using the *best-fit* parameters, we obtain the peak at $\simeq$ 1550 keV shown in the same Fig. 11 (light dashed line), which is absent in the experimental data for the reasons given above. A further test on the absence of such a peak is given by Fig. 7 where there is no evidence for α events at energies lower than 1600 keV. It follows that, in our case the ^{227}Ac ($T_{1/2} =$ 21.8 yr) can be considered as father isotope of the decay chain, while there are no traces of decays due to the first isotopes of the ^{235}U chain.

Let us now put forward some other considerations about this fact. At first [20] the chemistry of Lanthanides and Actinides is similar, so the U and Th content in Lanthanide minerals can be high: as example the Australian monazite, from which Lantanium can be derived, contains 6.7% of Th. Moreover, even if the decay chains would originally be in equilibrium, U and Th would be removed during the Lanthanide purification, but this procedure is not so efficient for some of the daughters; thus, a trace of U and Th can be kept in form of ^{227}Th, ^{223}Ra and daughters with a similar activity [20].

Moreover, using the value of the activity obtained by the α contamination analysis, we obtain here for the ^{227}Ac: $C_{^{227}Ac} = (6.7 \pm 0.3) \times 10^{-4}$ ppt. In the radioactive chain following ^{227}Ac are also present β decays from ^{227}Ac, ^{211}Pb and ^{207}Tl which contribute to the energy spectrum below 1600 keV. Assuming the chain in equilibrium after the ^{227}Ac, an activity similar as that due to the α decays can be considered also for these processes. In particular, the contribution from ^{227}Ac ($Q_\beta = 44$ keV) can be neglected (events under the used $\simeq$ 50 keV threshold). As regards the β decays of ^{211}Pb and ^{207}Tl, a simulation has allowed to obtain the expected energy distributions. These distributions are mainly due to the β decay in the ground state of the daughter nucleus. In a next section, their contribution will be taken into account together with that more consistent of ^{138}La to analyze the whole experimental energy spectrum below 1600 keV.

4.2. Contribution from ^{138}La

As mentioned above, the energy distribution measured by the $LaCl_3$:Ce detector below 1600 keV is dominated by the ^{138}La decays ($T_{1/2} = (1.05 \pm 0.03) \times 10^{11}$ yr [21]). Our crystal, (49.7 ± 1.3) g mass with a Ce concentration of (8.5 ± 1.0)%, contains $(1.01 \pm 0.04) \times 10^{20}$ nuclei of ^{138}La; thus, an activity of (21.1 ± 1.4) Bq can be derived.

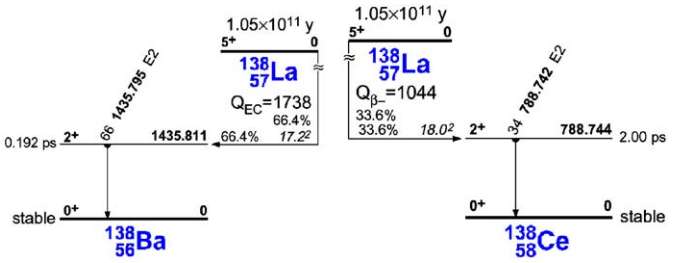

Fig. 12. Decay scheme of ^{138}La from Ref. [21]. The use of the more recent scheme in Ref. [22] would give results fully compatible within errors.

In Fig. 12 the ^{138}La decay scheme is shown. This isotope in $(66.4 \pm 0.5)\%$ of the cases decays by EC in ^{138}Ba, while in the remaining $(33.6 \pm 0.5)\%$ β decays in ^{138}Ce [21].

The expected energy spectrum due to ^{138}La decays has been simulated with the help of the EGS4 package and of a dedicated event generator.

The β decay ($Q_\beta = 1044$ keV) in ^{138}Ce is characterized by a unique emitted β (*end-point* $= 255$ keV) followed by a 789 keV deexcitation γ from the daughter nucleus. In the experimental data, the β decay gives rise to the β spectrum visible below $\sim$250 keV when the γ escapes the detector and to the structure between $\sim$800 and $\sim$1000 keV when the 789 keV γ is fully contained. Furthermore, around 600 keV the Compton edge of the γ summed to the β spectrum is also visible.

As regards the EC process, it is followed by a γ of $\simeq$ 1436 keV and X-rays/Auger electrons. In particular, in the $(63.5 \pm 0.5)\%$ an electron from shell K ($E_K \simeq 38$ keV) is involved, in the $(27.7 \pm 0.4)\%$ an electron from shell L ($E_L \simeq 6$ keV) and in $(8.86 \pm 0.14)\%$ an electron from upper shells. The EC process produces in the experimental spectrum the peak at $\simeq$ 1500 keV (sum of the 1436 keV γ and X-rays/Auger electrons) with its Compton edge at $\simeq$ 1250 keV and the X-rays/Auger electrons peaks in the low energy region due to the escape of the 1436 keV γ.

A devoted measurement ($T = 493$ h) has allowed to point out the peak at $\simeq$ 38 keV due to the shell K deexcitation and part of 6 keV peak due to shell L deexcitation and shaped by the energy threshold (see Fig. 10 left).

The peak at $\simeq$ 38 keV can also be used to evaluate the ^{138}La activity in the detector. Using the peak detection efficiency—accounting also for the branching ratio—obtained by the simulation: $\varepsilon_{peak} = 0.330 \pm 0.005$ (the error considers the uncertainties in the decay scheme) and the number of experimental counts due to the peak (fit of the experimental data): $N_{peak} = (1.203 \pm 0.005) \times 10^7$, the resulting activity of ^{138}La is: $a_{^{138}La} = N_{peak}/(\varepsilon_{peak} \times T) = (20.5 \pm 0.4)$ Bq. This result is well in agreement with the previous estimation from ^{138}La content in the crystal.

Another determination of the ^{138}La activity can be obtained analyzing the whole experimental energy spectrum below 1600 keV. Here, the expected distribution is due to the sum of the contributions from β decays of ^{211}Pb and ^{207}Tl (whose activity has been determined above) and of that more consistent of ^{138}La. The expected energy distribution has been fitted to the experimental energy spectrum in order to estimate the ^{138}La contribution; the only free parameter is the number of events due to ^{138}La contribution: $N = (5.23 \pm 0.10) \times 10^6$ events, thus for an exposure of $T = 70.2$ h it results in activity for ^{138}La: $a_{^{138}La} = N/T = (20.7 \pm 0.4)$ Bq, in agreement with the previous estimates.

Finally, our evaluation of the $T_{1/2}$ of ^{138}La can be derived from the measured activity: $a_{^{138}La} = \ln 2 \times N_{^{138}La}/T_{1/2}$, thus, considering the number of ^{138}La nuclei in the detector it follows: $T_{1/2} = \ln 2 \times N_{^{138}La}/a_{^{138}La} = (1.07 \pm 0.06) \times 10^{11}$ yr, well compatible with previous experimental estimation: $T_{1/2} = (1.05 \pm 0.03) \times 10^{11}$ yr [21].

4.3. Conclusions

In conclusion, Fig. 13 shows the comparison between the experimental energy spectrum (continuous histogram) and the full simulation contributions (dashed line). A good agreement has been obtained.

5. An example of application: results on some cluster decay modes in ^{138}La and ^{139}La

The spontaneous emission of nuclear fragments heavier than α particles and lighter than the most probable fission fragments, named cluster decay, was theoretically predicted in 1980 [23] and experimentally observed for the first time in 1984 [24,25]. Up to date, spontaneous emissions of clusters ranging from ^{14}C to ^{34}Si from near 20 translead nuclei (from ^{221}Fr to ^{242}Cm) have been observed [26,27]. In all these decays double magic nucleus ^{208}Pb, or nuclei close to ^{208}Pb, are produced allowing to consider this domain of cluster decays as "lead radioactivity" [27], analogously to "α radioactivity".

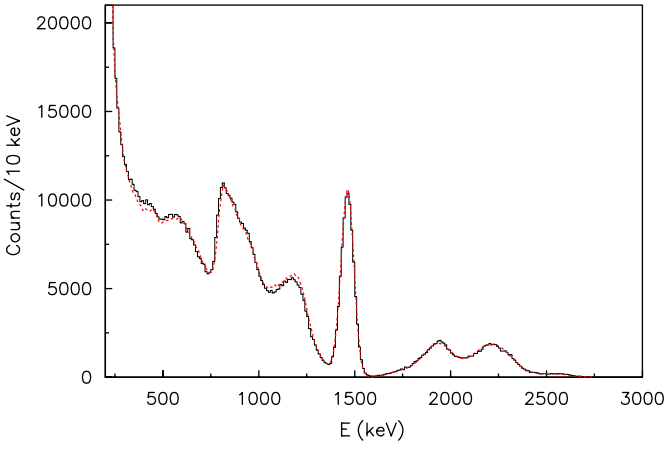

Fig. 13. Comparison between the experimental energy distribution (continuous histogram) and simulation (dashed line) (see text).

A new region of parent nuclei, for which cluster radioactivity can experimentally be observed, was predicted recently in Ref. [28]: these are the nuclei with $Z = 56 - 64$ and $N = 58 - 72$; daughter nuclei are close to double magic $^{100}_{50}$Sn. In Ref. [29] we have already investigated several possible cluster decays of ^{127}I.

Here we will use the exposure collected deep underground with the $LaCl_3$:Ce detector in order to investigate some of the possible cluster decay modes in ^{138}La and ^{139}La.

It is worth to note that theoretical calculations for the half-lives of ^{138}La and ^{139}La cluster decays, based on analytical superasymmetric fission model [30], were pessimistic. Recently, several semiempirical formulae for the calculation of $T_{1/2}$ in cluster decays have been proposed [31–33] with numerical parameters determined by fitting the known experimental data. However, despite these formulae work nicely in the region of "lead radioactivity" [27], they give very discrepant results when applied to cluster decay of ^{138}La or ^{139}La: calculated $T_{1/2}$ differ by orders of magnitude (see Table 1). Such a discrepancy gave us additional motivation for the experimental investigation of the ^{138}La and ^{139}La cluster decays.

In the present case the ^{138}La and ^{139}La parent nuclei are incorporated in the $LaCl_3$:Ce detector itself (natural abundance of ^{138}La and ^{139}La are 0.0902% and 99.9098%, respectively) and the subsequent decays of the created clusters (which are usually radioactive) are searched for. In fact, all the nuclides listed in Table 1 are radioactive with the exception of ^{48}Ca which is unstable to $2\beta2\nu$ decay mode, but with very high $T_{1/2} \simeq 4.3 \times 10^{19}$ yr [35]. Thus, for each considered decay channel, the data analysis has been realized here searching for the signals produced in the subsequent decay chain of the nuclides in the cluster.

In Fig. 14 we show the decay chains just for the three cluster decay processes analysed in the present paper.

For each process a Monte Carlo estimate of the expected signal energy distribution has been calculated on the basis of the EGS4 code [14] and of a dedicated event generator. It is worth to note that time correlation analyses (as e.g. we did in Ref. [29]) would not add here more information because of the lifetimes of the involved nuclides and of the high background level of the $LaCl_3$:Ce crystal.

Table 1
Possible decay branches for ^{138}La and ^{139}La; in all these cases doubly magic nucleus ^{48}Ca (or nuclei in neighborhood of ^{48}Ca) is emitted

Decay	Q (MeV)	$T_{1/2}$ (yr)		
	[34]	[31]	[32]	[33]
^{138}La → ^{48}Ca + ^{90}Rb	37.05	3.8×10^{85}	5.5×10^{13}	4.2×10^{44}
^{138}La → ^{49}Ca + ^{89}Rb	36.48	3.8×10^{88}	6.7×10^{13}	1.2×10^{46}
^{138}La → ^{50}Sc + ^{88}Kr	37.70	7.3×10^{88}	6.8×10^{5}	1.3×10^{46}
^{139}La → ^{48}Ca + ^{91}Rb	34.73	2.2×10^{94}	3.4×10^{17}	1.3×10^{52}
^{139}La → ^{50}Ca + ^{89}Rb	34.05	1.0×10^{99}	1.2×10^{17}	9.7×10^{53}
^{139}La → ^{51}Sc + ^{88}Kr	35.68	2.6×10^{97}	1.3×10^{8}	5.7×10^{52}
^{139}La → ^{54}Ti + ^{85}Br	36.97	3.1×10^{98}	1.7×10^{-2}	1.3×10^{52}
^{139}La → ^{55}V + ^{84}Se	37.87	7.3×10^{98}	7.6×10^{-12}	1.4×10^{52}

In this paper in particular we evaluate new experimental limits just for the first, fourth and sixth listed decay processes.

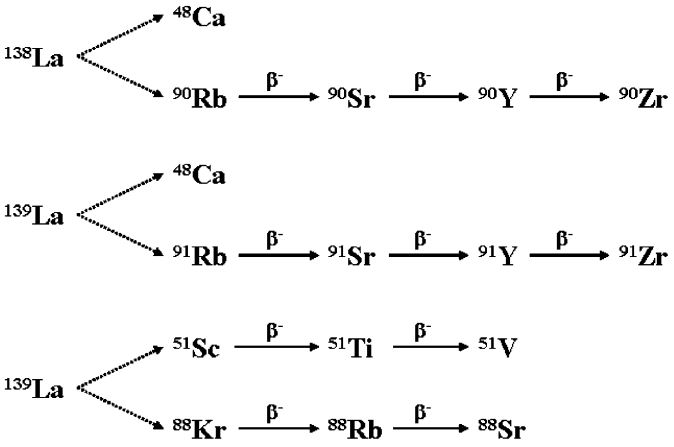

Fig. 14. Decay chains that follow the three cluster decay processes analysed in the present paper. We remind that ^{48}Ca is unstable to $2\beta2\nu$ decay mode, but with very high $T_{1/2} \simeq 4.3 \times 10^{19}$ yr [35].

As it can be seen, still significant part of the expected energy distributions in Fig. 15 remains above 2.83 MeV, that is in the region where zero counts have been measured during 70.2 h; thus, we focus our attention on the energy region above 2.83 MeV. As a consequence, the measured upper limit on signal events in the considered energy region is 2.3 counts (90% C.L.), according to the procedure of Ref. [19] for each considered process. Then, we calculate the number of events (per 1 decay) detected above 2.83 MeV for each cluster decay, η; it is worth to note that one cluster decay can give rise to more than a single detected event. Using the standard formula $T_{1/2} = \ln 2\,(N \times T/N_d)$ with N number of atoms of ^{138}La or of ^{139}La, T running time and $N_d < 2.3/\eta$ number of events which can be ascribed to the process searched for, one obtains the results summarized in Table 2.

The obtained limits exclude application of semi-empirical formulae of Ref. [32] for cluster radioactivity in investigated nuclear region.

6. Conclusion

The features of a $LaCl_3$:Ce detector have been investigated deep underground for the first time. An investigation of time correlated events, such as α–α and Bi–Po events, and a study of the experimental energy distribution have been carried out and have allowed e.g.: (i) to determine the α/β light ratio in the used detector; (ii) to investigate the α/β pulse shape discrimination capability; (iii) to quantify the main radioactive contaminants of the detector. As an example of possible application a search for some possible

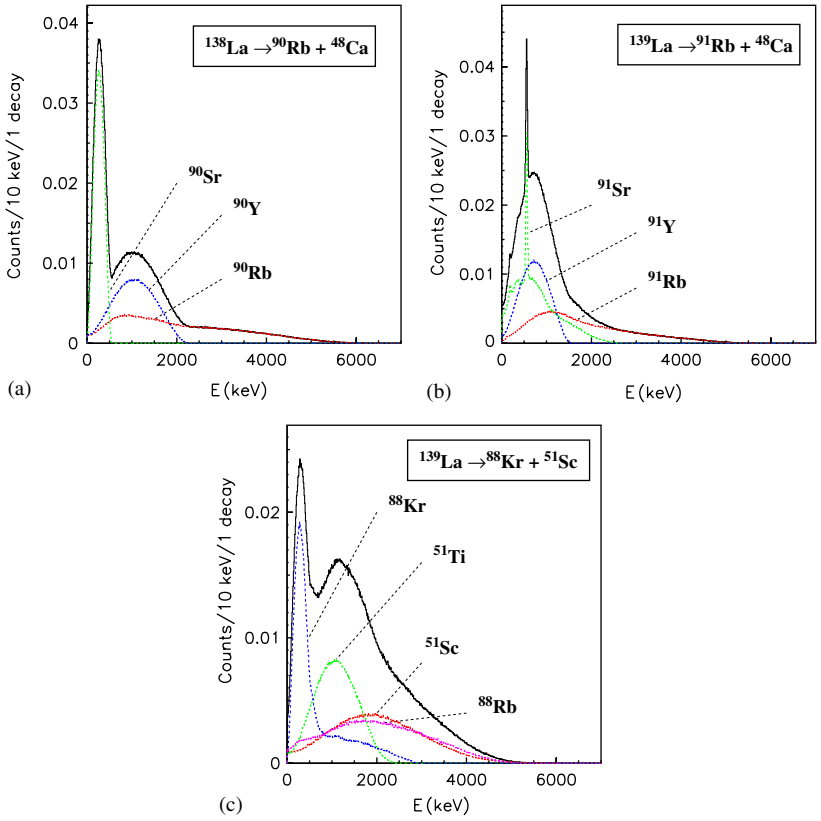

Fig. 15. Expected energy distributions for the three possible cluster decays considered in the present paper.

Table 2
New experimental lower limits (90% C.L.) on $T_{1/2}$ obtained for the quoted cluster decays of ^{138}La and ^{139}La

Decay	η	N_d (90% C.L.)	$T_{1/2}$ (yr) (90% C.L.)
^{138}La → ^{48}Ca + ^{90}Rb	0.286	<8.0	$>7.0 \times 10^{16}$
^{139}La → ^{48}Ca + ^{91}Rb	0.187	<12.3	$>5.0 \times 10^{19}$
^{139}La → ^{51}Sc + ^{88}Kr	0.461	<5.0	$>1.2 \times 10^{20}$

The η values are the number of events (per 1 decay) detected above 2.83 MeV for each cluster decay; it is worth to note that one cluster decay can give rise to more than a single detected event. Moreover, $N_d < 2.3/\eta$ are the upper limits (90% C.L.) on the number of cluster decays searched for; see text.

cluster decays modes in La isotopes has been carried out setting new experimental limits.

Due to the high ^{138}La content in natural La and to the presence of daughters from the broken ^{235}U chain, an extensive application of $LaCl_3$:Ce in the search for rare processes appears at present difficult, remaining however this kind of scintillator potentially very competitive for some sea level applications.

Acknowledgements

Authors acknowledge useful discussion with F.A. Danevich.

References

[1] K.S. Shah, et al., Nucl. Instr. and Meth. A 505 (2003) 76.
[2] Saint Gobain crystals & detectors, "$LaCl_3$:Ce data sheet".
[3] E.V.D. van Loef, et al., Appl. Phys. Lett. 77 (2000) 1467.
[4] O. Guillot-Noel, et al., J. Lumin. 85 (1999) 21.
[5] J.K. Hartwell, R.J. Gehrke, Applied Rad. and Isotopes 63 (2005) 223.
[6] J. Andriessen, et al., Optics Commun. 178 (2000) 355.
[7] M. Balcerzyk, et al., Nucl. Instr. and Meth. A 537 (2005) 50.
[8] R. Bernabei, et al., Il Nuovo Cimento A 110 (1997) 189.
[9] P. Belli, et al., Astrop. Phys. 10 (1999) 115.
[10] P. Belli, et al., Nucl. Phys. B 563 (1999) 97.
[11] R. Bernabei, et al., Nucl. Phys. A 705 (2002) 29.
[12] P. Belli, et al., Nucl. Instr. and Meth. A 498 (2003) 352.
[13] R. Cerulli, et al., Nucl. Instr. and Meth. A 525 (2004) 535.
[14] W.R. Nelson, et al., SLAC-265, UC-32 (E/I/A).
[15] Saint Gobain crystals & detectors, private communication.
[16] E. Gatti, F. De Martini, Nuclear Electronics, vol. 2, IAEA, Vienna, 1962, p. 265.
[17] C. Hoel, et al., Nucl. Instr. and Meth. A 540 (2005) 205.
[18] M. Balcerzyk, et al., Nucl. Instr. and Meth. A 537 (2005) 50.
[19] K. Hikasa, et al., Phys. Rev. D 45 (1992) III.32.
[20] G. Gautier, et al., Presented at IEEE conference, 2005.

[21] J.K. Tuli, Nucl. Data Sheets 74 (1995) 349.
[22] A.A. Sonzogni, Nucl. Data Sheets 98 (2003) 515.
[23] A. Sandulescu, et al., Sov. J. Part. Nucl. 11 (1980) 528.
[24] H.J. Rose, G.A. Jones, Nature 307 (1984) 245.
[25] D.V. Aleksandrov, et al., JETP Lett. 40 (1984) 909.
[26] R. Bonetti, A. Guglielmetti, in: W. Greiner, R.K. Gupta (Eds.), Heavy elements and related new phenomena, vol. 2, World Scientific, Singapore, 1999, p. 643.
[27] S.P. Tretyakova, et al., Prog. Theor. Phys. Suppl. 146 (2002) 530.
[28] D.N. Poenaru, et al., Phys. Rev. C 47 (1993) 2030.
[29] R. Bernabei, et al., Eur. Phys. J. A 24 (2005) 51.
[30] D.N. Poenaru, et al., Atom. Data Nucl. Data Tables 34 (1986) 423.
[31] D.N. Poenaru, et al., Phys. Rev. C 65 (2002) 054308.
[32] M. Balasubramaniam, et al., Phys. Rev. C 70 (2004) 017301.
[33] Z.Z. Ren, et al., Phys. Rev. C 70 (2004) 034304.
[34] G. Audi, et al., Nucl. Phys. A 729 (2003) 337.
[35] A. Balysh, et al., Phys. Rev. Lett. 77 (1996) 5186.